PAPER

Universal quantum state preparation via revised greedy algorithm

Quantum Science and Technology

PAPER

Universal quantum state preparation via revised greedy algorithm

RECEIVED
27 April 2021

REVISED
1 August 2021

ACCEPTED FOR PUBLICATION
16 August 2021

PUBLISHED
3 September 2021

Run-Hong He, Hai-Da Liu, Sheng-Bin Wang, Jing Wu, Shen-Shuang Nie and Zhao-Ming Wang*

College of Physics and Optoelectronic Engineering, Ocean University of China, Qingdao 266100, People's Republic of China
* Author to whom any correspondence should be addressed.

E-mail: mingmoon78@126.com

Keywords: quantum state preparation, semiconductor double quantum dots, superconducting circuits, dynamic control pulses

Abstract

Preparation of quantum state lies at the heart of quantum information processing. The greedy algorithm provides a potential method to effectively prepare quantum state. However, the standard greedy (SG) algorithm, in general, cannot take the global maxima and instead becomes stuck on a local maxima. Based on the SG algorithm, in this paper we propose a revised version to design dynamic pulses to realize universal quantum state preparation, i.e. preparing an arbitrary state from another arbitrary one. As applications, we implement this scheme to the universal preparation of single- and two-qubit state in the context of semiconductor quantum dots and superconducting circuits. Evaluation results show that our scheme outperforms the alternative numerical optimizations with higher preparation quality while possesses the comparable high efficiency. Compared with the emerging machine learning, it shows better accessibility and does not require any training. Moreover, the numerical results show that the pulse sequences generated by our scheme are robust against various errors and noises. Our scheme opens a new avenue of optimization in few-level system and limited action space quantum control problems.

1. Introduction

Benefited from the fascinating abilities afforded by the quantum mechanics, quantum computers of the future are supposed to tackle specific tasks that are intractable or even prohibitive to solve with their classical counterparts [1–8]. Over the past few decades, a wide variety of physical modalities has been proposed theoretically and demonstrated experimentally to construct the prototypes of quantum computers, spanning from a single electron to the topological system [9–16]. Along with the mature of the hardware, the task of designing control trajectory partially falls on the programming side which bridges quantum science and traditional disciplines.

It has been proved that with only arbitrary single-qubit rotations on the Bloch sphere plus an entangling two-qubit gate, arbitrary quantum logic can be performed on a gate-based quantum computer, or rather, they are universal [1]. Various scenarios have discussed how to decompose a quantum algorithm into an arrangement of these universal gates [1, 17–19]. Meanwhile, it has also been explored how to construct optimal gate synthesis with the universal gate set for general logical operation [20]. While, for a given experimental platform, there are always certain gates that are more efficient to implement than others, or even the key ingredients of the latter. Thus, they are often referred to as 'native gates' of that platform. To enact quantum computation, it is required to decompose a given quantum algorithm into a sequence of discrete native gates according to the underlying hardware properties [21, 22].

Experimentally, these native gates are performed by electromagnetic pulses with precise amplitudes and durations. However, the difficulty of scheduling these pulses to implement a logical gate sharp increases with the decrease of the degrees of freedom in general. A prominent example is the pluses designing for a singlet–triplet (S–T_0) qubit in a semiconductor double quantum dot (DQD). Where the only tunable parameter is the exchange coupling between two trapped electrons, which associates with the rotation rate

about the z-axis of the Bloch sphere. The process of designing pulses analytically requires to solve iteratively a set of nonlinear equations [23–25]. Thus it is an overhead costly and time-consuming task in practice. In order to improve efficiency, reference [26] discussed design pulses with supervised learning to get an approximation of that analytical solution. Considering the challenge to realize pulses with continuous intensity and duration in experiment, reference [27] employed deep reinforcement learning [28–31] to explore the preparation of a specific state from another one with dynamic pulses whose intensity and duration are both discrete, yet at the expense of universality. Respecting the virtues of discrete control, reference [32] studied the preparation of a certain state from an arbitrary state. In contrast, reference [33] promised to prepare an arbitrary state from a specific state in a multi-level nitrogen-vacancy center system. It is a meaningful point that by combining references [32, 33] the driving between any states can be implemented as suggested in reference [32]. In addition, it is also a promising direction to train the network with both random initial state and target state to achieve the same objective directly. Except for the nascent machine learning, there are also several sophisticated versatile optimization approaches based on gradient can be utilized, such as stochastic gradient descent [34], gradient ascent pulse engineering (GRAPE) [35, 36] and chopped random-basis optimization (CRAB) [37, 38]. They have been successfully applied to a wide array of optimization problems. While, suffering from the sensitivity to the initial control trajectory setting, in general, they can find only local maxima, instead of global maxima, and quit the iterative process with an inadequate fidelity.

In this paper, based on the standard greedy (SG) algorithm [39, 40], a common technology for optimization, we provide an improved version, i.e. revised greedy (RG) algorithm to drive an arbitrary state to another arbitrary state, or say, universal state preparation with discrete control. On the one hand, differing from the algorithms based on the machine learning, which suffers from the long hours of training and the resulting huge computational overhead, our scheme needs no training at all, which ensures high accessibility. On the other hand, contrasting to the traditional optimization methods, our scheme overcomes the local optimality and achieves a higher preparing quality. In addition, compared with them, the average runtime of identifying the appropriate pulses with our scheme is comparable to the GRAPE, which is known for its high efficiency. We apply our scheme exemplarily to the universal single- and two-qubit state preparation in the context of S–T_0 spin qubits in semiconductor DQDs and superconducting quantum circuits Xmon qubits [41, 42]. Our method is general enough to be extended to varieties of few-level system and limited action space quantum control problems.

The remainder of this paper is organized as follows. In section 2, we describe in detail the method used in this work. Then we present the results in section 3, and conclude in section 4. The models considered in this paper are collected in section 5.

2. Method

Dynamic programming, an important member of the optimization theory, divides a complex problem into multiple simple sub-problems, and then solves each sub-problem individually. It is expert in solving the Markov decision process, in which the resulting state S' is determined uniquely by the current state S and the action a taken by the agent while has no connection with the history of the system [43]. The SG algorithm, which is built upon the dynamic programming, approximates the global result by collecting the optimal solutions of each sub-problem [39, 40]. The SG algorithm as well as its variants is the most commonly used strategy to determine which action to explore in a given state in optimizations and acts as a crucial ingredient in many successful quantum control schemes, such as the designing of high-fidelity quantum gates [44, 45] and the scheduling of quantum gates to implement quantum algorithm [46]. However, because of the overemphasis on local optimality, in general, the SG algorithm cannot produce the global maxima. In order to overcome the local optimality of the SG algorithm, we propose here a revised version, i.e. the RG algorithm to design the control pulses.

Our target is to design pulses to drive an arbitrary given quantum state to another arbitrary state. To illustrate the process of designing pulses clearly, we consider exemplarily the driving from the initial state $|S_0\rangle = |0\rangle$ to the target state $|S_{\rm tar}\rangle = |1\rangle$ with single-parameter dynamic pulses. The quality of the state preparation is evaluated by the fidelity, which is defined as $F \equiv |\langle S_{\rm tar}|S_n\rangle|^2$, where $|S_n\rangle$ (also noted as S_n for simplicity) refers to the evolution state at time step n. The schematic of this processing is patterned in figure 1. To reduce the computational overhead, the control function is discretized as a piecewise constant pulse-sequence [36]. The maximum evolution time T is divided uniformly into N slices with pulse duration $\mathrm{d}t = T/N$. All of the allowed actions adopted in this work accommodate the fundamental constraints and experimental realities, such as pulse height, duration, etc [47–49]. This control function can be readily implemented with suitable electrodes voltages generated by an arbitrary waveform generator in the platform of semiconductor QDs [50]. While, for the control of superconducting circuits, these pulses with

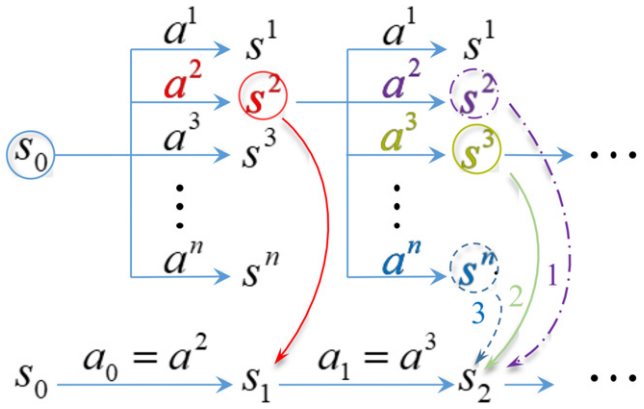

Figure 1. Schematic of the RG algorithm for control trajectory designing. The details of this algorithm are described in the main text of section 2 and in the pseudocode algorithm 1.

Algorithm 1. Pseudocode of the RG algorithm for control trajectory designing.

Initialize the time step step $=0$ and state s_{step} according to the testing point.
Calculate the fidelity F_{step} and make $F_{\max} = F_0 = F_{\text{step}}$.
while True **do**
Perform the allowed actions a^i separately and record the corresponding fidelity F^i.
If $\max(F^i) > F_{\text{step}}$, let $F_{\text{step}+1} \leftarrow \max(F^i)$, specify the corresponding action $a_{\text{step}} = \text{argmax}_{a^i} F^i$ as the '*best action*' in this time step and make $F_{\max} \leftarrow F_{\text{step}+1}$.
Else, assign the '*best action*' (strategy 1) or '*next-best action*' (strategy 2) or '*worst action*' (strategy 3) as the '*selected action*' a_{step} and record the corresponding fidelity as $F_{\text{step}+1}$.
Next state $s_{\text{step}+1}$ are the state caused by performing the '*selected action*'.
Let $s_{\text{step}} \leftarrow s_{\text{step}+1}$ and step $=$ step $+ 1$.
Break if step $\geqslant$ step$_{\max}$ or $F > 0.999$.
end while
Output $F_{\max}$ as the maximum fidelity and the action sequence composed of the '*selected actions*' from step $= 0$ to the step$_{\text{end}}$ in which we take the $F_{\max}$.

discrete intensity and duration can be translated into continuous microwaves generated by a typical IQ modulation setup [49]. Presume there are four allowed actions $\{a^1, a^2, a^3, a^4\}$ corresponding to four allowed pulse strengths respectively.

The scheme goes as follows: initially, the fidelity of the state S_0 is $F_0 = 0$. Then, calculate each fidelity F^i caused by the corresponding action a^i after dt evolution. We assume these resulting fidelities are 0.1, 0.3, 0.2, 0.15 respectively, and all of them are bigger than F_0. Then we choose the maximum of F^i as the fidelity at this time step, i.e. $F_1 \rightarrow F^2 = 0.3$; the corresponding action as the 'selected action', $a_0 \leftarrow a^2$; and the corresponding evolution state as the next state, $S_1 \leftarrow S^2$. This step dovetails neatly with the SG algorithm: employ directly the 'best action'. After, based on the state S_1, perform the allowed actions a^i separately again and take the corresponding fidelities F^i. Assume the resulting fidelities are 0.26, 0.3, 0.28 and 0.25 respectively, and obviously there's no new fidelity bigger than F_1. To overcome the local optimality in this case, we employ three strategies to decide which action should be selected: **strategy 1**, choose the 'best action' according to the greedy algorithm; **strategy 2**, the 'next-best action'; and **strategy 3**, the 'worst action'. And repeat the above operations, until the final time step N or the fidelity exceeds a certain satisfactory threshold. Note that in an episode, from the first step to the last, only one strategy is adopted to ensure the stability of the algorithm. Finally, take the action-sequence as the solution corresponding to the strategy in which we obtained the maximum fidelity. For current computer, with more than enough CPU cores available, these strategies can be readily executed on different processings in parallel, making it an extremely effective algorithm. The pseudocode of this RG algorithm is given in algorithm 1.

The core of this scheme lies at the introduction of deliberate perturbation, represented as the selection of 'non-best' action, when the state are stuck on local maxima, which is regarded empirically as an efficient way to achieve a better performance [36]. This setting is necessary for cases like that: with the north pole of Bloch sphere targeted, the 'best' action may always orient the state located in the equator along the equator and cannot reach a better place forever. In addition, unlike algorithms based on machine learning, there's no training at all. Alternatively, the RG explores the suited action as well as the next state by trials and errors online, converting a complicated model-free environment into a simple model-based one which the

algorithm fully understands [43]. So that it does not require learning of the environment and actions any more.

Our scheme achieves a better performance than the comparable approaches in few-level system and limited action space quantum control problems, such as the single- and two-qubit state preparation as we will demonstrate in the following section. Nonetheless, this advantage may diminish as the number of qubits and the action space blow up, partially due to the huge increase in them will limit this method's efficiency. (For optimization problems with continuous action space, the machine learning certainly has more natural advantages.) In addition, in many-body preparation, such as the quantum state transfer, there may be a lack of a well metric to determine which state is 'better' than others in the intermediate process. One possible route for improvement is to use this method in concert with other algorithms, which we leave as future works. However, even if the many-body state preparation is a very important topic from the application point of view, as we mentioned in the introduction, with only arbitrary single- and two-qubit gates, any quantum logic can be implemented on a circuit-model quantum computer.

3. Results

In the preceding section, we have presented the method used in this work. Now, we consider four cases of state preparation: single- and two-qubit state preparation in the context of semiconductor DQDs or superconducting circuits. The details of the models are introduced in section 5.

Any single-qubit state can be graphical represented by a point on the Bloch sphere

$$|\Psi(\theta,\varphi)\rangle = \cos\left(\frac{\theta}{2}\right)|0\rangle + e^{i\varphi}\sin\left(\frac{\theta}{2}\right)|1\rangle, \tag{1}$$

where the polar angle $\theta \in [0,\pi]$ and the azimuthal angle $\varphi \in [0,2\pi)$ [1]. To verify the universality, for the single-qubit state preparation, we sample 128 testing points on the Bloch sphere, which is distributed uniformly at the angles θ and φ.

For the two-qubit state preparation, we take a data set comprising 6912 points which are defined as $\{[a_1,a_2,a_3,a_4]^{\mathrm{T}}\}$, where $a_j = e^{i\phi}c_j$ refers to the probability amplitude of the jth basis state, with $\phi \in \{0,\pi/2,\pi,2\pi/3\}$; and these c_js together indicate the coordinates of points scattered on a four-dimensional unit hypersphere

$$\begin{cases} c_1 = & \cos\theta_1, \\ c_2 = & \sin\theta_1\cos\theta_2, \\ c_3 = & \sin\theta_1\sin\theta_2\cos\theta_3, \\ c_4 = & \sin\theta_1\sin\theta_2\sin\theta_3, \end{cases} \tag{2}$$

with $\theta_i \in \{\pi/8,\pi/4,3\pi/8\}$ [32]. While, to reduce the overhead, we select randomly 512 samples from that data set to form the testing set in this case.

Each point in the testing set will be prepared as target state from all other points in turn. And then the average fidelity $\overline{F}$ of each target state preparation can be taken. The universality is evaluated by the mean of these average fidelities $\langle\overline{F}\rangle$ over all target states: for the cases of single-qubit state preparation, there are $128\times(128-1) = 16\,256$ preparation tasks. For the two-qubit cases, the total number of tasks is 261 632.

3.1. Universal single-qubit state preparation with revised greedy algorithm

Arbitrary manipulations of a single-qubit state can be achieved by successive rotations on the Bloch sphere, which are completed by a sequence of control pulses [25]. The only tunable parameter of single-qubit in S–T_0 DQD is the coupling strength $J(t)$, which is bounded physically to be non-negative and finite. Here, we take four discrete allowed actions, i.e. $J \in \{0,1,2,3\}$, to drive single-qubit states.

In Xmon superconducting circuits system, the drives on x- and y-directions are limited to be finite, while the drive on z-direction is further restricted to be non-negative. We choose 11 discrete allowed actions $A_{x(y)} \in \{-2,-1,0,1,2\}$, $A_z \in \{0,1,2\}$ and within a time step we just take the action A_x, A_y or A_z alone.

The results of state preparation under different control parameters in two models are captured and shown in table 1. For visualization, figures 2(a) and (b) plot the average preparation fidelity $\overline{F}$ of each single-qubit target state parameterized by angles θ and φ in the context of semiconductor DQD and superconducting circuits respectively. The data correspond to the second and tenth rows of the table 1, respectively. In figure 2(a), we can see that, although there's only one degree of freedom, the fidelities of state preparation are high in most areas. Whereas there also some 'bad points' exist and cluster together that

Table 1. List of parameters and the corresponding average fidelity over all sampled state preparation tasks in four cases.

Model	Qubit	T	dt	$\langle\overline{F}\rangle$
DQDs	Single-	π	$\pi/10$	0.951
		2π	$\pi/5$	0.973
		3π	$\pi/3$	0.977
		4π	$\pi/3$	0.983
		5π	$\pi/2$	0.894
	Two-	10π	$\pi/2$	0.911
		15π	$\pi/2$	0.930
		20π	$\pi/2$	0.938
Superconducting circuits		π	$\pi/3$	0.983
	Single-	π	$\pi/5$	0.999
		π	$\pi/10$	0.998
		π	$\pi/20$	0.999
		5π	$\pi/4$	0.964
	Two-	10π	$\pi/4$	0.971
		12π	$\pi/4$	0.975
		15π	$\pi/4$	0.977

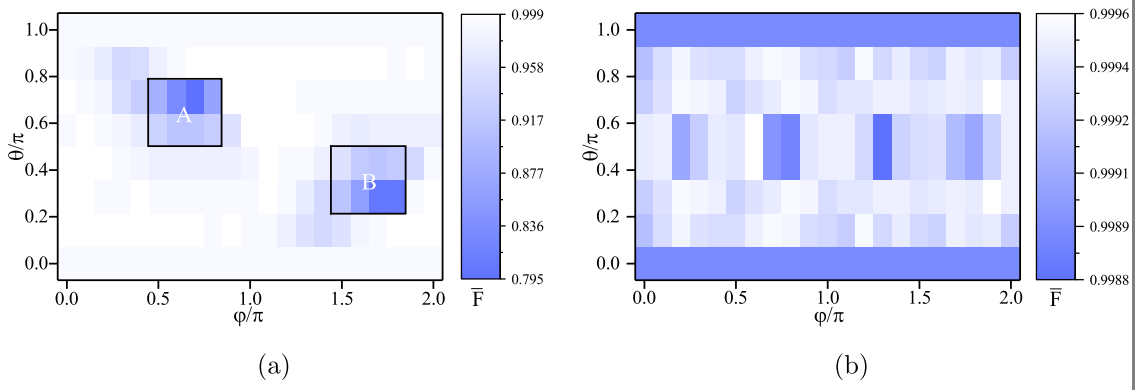

Figure 2. Average fidelities $\overline{F}$ distribution of preparing arbitrary single-qubit target state $\Psi(\theta, \varphi)$ using RG algorithm over 127 sampled tasks. (a) The mean of all average fidelities $\langle\overline{F}\rangle = 0.973$ in DQDs system with $T = 2\pi$ and d$t = \pi/5$. The areas A and B are clustered bad points whose mean of average fidelities $\langle\overline{F}\rangle$ are 0.902 and 0.886 respectively. (b) The mean of all average fidelities $\langle\overline{F}\rangle = 0.999$ in superconducting circuits system with $T = \pi$ and d$t = \pi/5$.

cannot reach the target states well, e.g. the areas A and B, where the corresponding $\langle\overline{F}\rangle = 0.902$ and 0.886, respectively. We ascribe this partially to the inappropriate parameter choice and believe it can be improved by further specifically tailoring parameters in these areas such as extended evolution time, altered action duration or more allowed actions. For example, leaving the other parameters intact, when $T = 8\pi$, d$t = \pi/3$, $\langle\overline{F}\rangle = 0.992$ in both the A and B areas. In contrast, benefited from the additional degrees of freedom in x- and y-axes, the performance of state preparation in superconducting circuits is much better than in DQD, as shown in figure 2(b), whose $\langle\overline{F}\rangle = 0.999$ and the minimum $\overline{F}$ still exceeds 0.998.

In addition, for comparing the performance of our scheme with the traditional optimization approaches, we plot the fidelities versus the corresponding runtime of designing pulses of our scheme plus the GRAPE, CRAB and SG for state preparation in DQDs and superconducting circuits in figures 3(a) and (b) respectively, of which the control parameters are identical to that adopted in figure 2. To ensure a fair comparison, for GRAPE and CRAB, we discretize their continuous control strengths to the nearest allowed actions at the end of the execution to get the final solution. It can be seen that, our RG algorithm outperforms the GRAPE, CRAB, and SG with higher quality of state preparation in both S–T_0 DQD and Xmon superconducting single-qubit models. While, the runtime of designing proper control trajectory is in the same order of magnitude as the sophisticated GRAPE, which is known for high efficiency.

It is worth stating that, the reasons are different for the diversity of designing time in different algorithms: the runtime of GRAPE and CRAB are mainly brought about by the number of iterations; while the runtime of SG and RG are mainly caused by the minimum time steps to finish an episode. That is, the time steps in GRAPE and CRAB are fixed—$N = T/$dt; yet the time steps in SG and RG are alterable, which may be smaller than N only if the requirement to terminate the episode early is met. (See the details of the RG described in section 2.) The RG favors a shorter path on the Bloch sphere between the initial and target

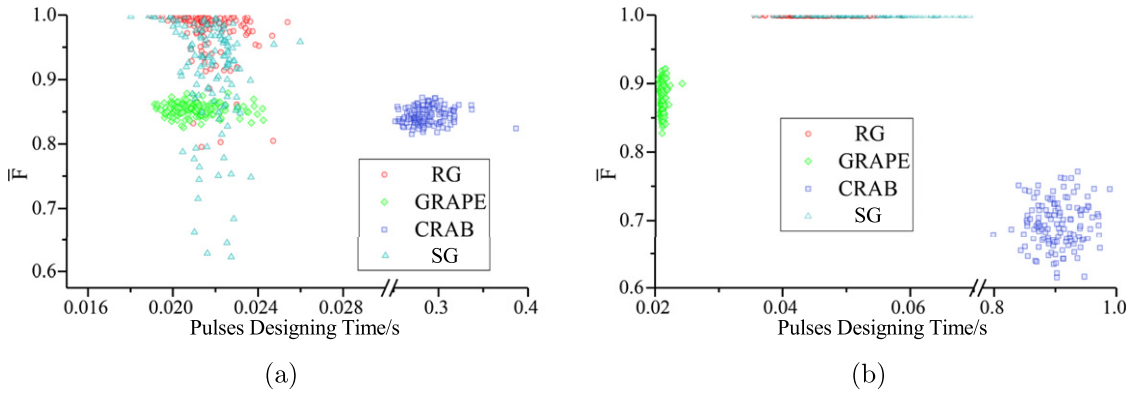

Figure 3. Average fidelities $\overline{F}$ versus designing time distributions of preparing arbitrary single-qubit target state over 127 sampled tasks with different optimization algorithms. The control parameters are identical to that adopted in figure 2. (a) State preparation in S–T_0 DQD, where the mean of all average fidelities $\langle\overline{F}\rangle = 0.972\,73, 0.853\,72, 0.844\,07, 0.911\,43$ and the mean of all average designing time $\langle\overline{t}\rangle = 0.0217, 0.0211, 0.2877, 0.0217$ with RG, GRAPE, CRAB and SG. (b) States preparation in Xmon superconducting circuits, where the mean of all average fidelities $\langle\overline{F}\rangle = 0.999\,44, 0.878\,07, 0.694\,25, 0.999\,37$ and the mean of all average designing time $\langle\overline{t}\rangle = 0.0449, 0.0214, 0.9050, 0.0520$ with RG, GRAPE, CRAB and SG.

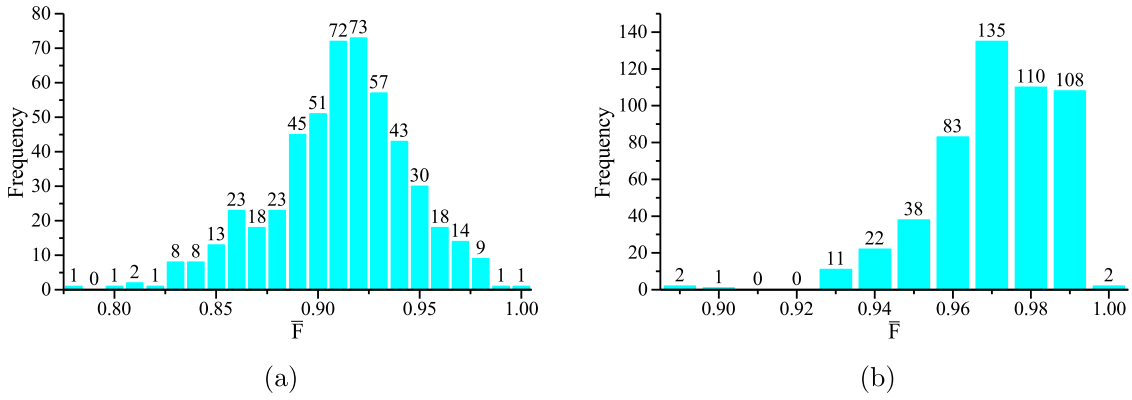

Figure 4. The frequency distributions of average fidelities $\overline{F}$ for two-qubit state preparation using RG algorithm over 511 sampled tasks. (a) The mean of all average fidelities $\langle\overline{F}\rangle = 0.911$ in DQDs system with $T = 10\pi$ and $\mathrm{d}t = \pi/2$. (b) The mean of all average fidelities $\langle\overline{F}\rangle = 0.971$ in superconducting circuits system with $T = 10\pi$ and $\mathrm{d}t = \pi/4$.

states compared to other algorithms. Whereas, geometrically, this discrete control does not suffice to hit the quantum speed limit. We intend to make another improved version of the SG utilizing pulses with continuous strength and duration to explore the speed limit of the similar quantum control problems in the future works.

3.2. Universal two-qubit state preparation with revised greedy algorithm

The control space for two-qubit state preparation in semiconductor DQDs is parameterized by the allowed pulse strengths in each qubit, i.e. $\{(J_1, J_2)|J_1, J_2 \in \{1, 2, 3, 4, 5\}\}$. Thus, there are $5 \times 5 = 25$ allowed actions. As for two-qubit states preparation in superconducting circuits, the allowed actions on each qubit are same as these taken in the single-qubit case. The total number of allowed actions is $11 \times 11 = 121$.

The detailed control parameters and the corresponding results in two models are listed in table 1. Meanwhile, figures 4(a) and (b) plot the frequency distributions of average preparation fidelity $\overline{F}$ of each target point over sampled tasks in semiconductor DQDs and superconducting circuits, respectively. We can see that as an optimization method with low computational overhead, even in the case of lack of degrees of freedom, it still performs well in some certain points. It is worth pointing out that again each $\overline{F}$ of target point is over 511 preparation tasks, thus a high-valued $\overline{F}$ implies hundreds of successes of precise state preparation tasks. While these bad points can also perform better, in general, by carefully selecting parameters as it is in the case of single-qubit. For example, if the 'worst point' in figure 4(a) (whose $\overline{F} = 0.779$, under $T = 10\pi$ and $\mathrm{d}t = \pi/2$) is performed under $T = 18\pi$ and $\mathrm{d}t = \pi/2$, its $\overline{F}$ can also reach 0.813.

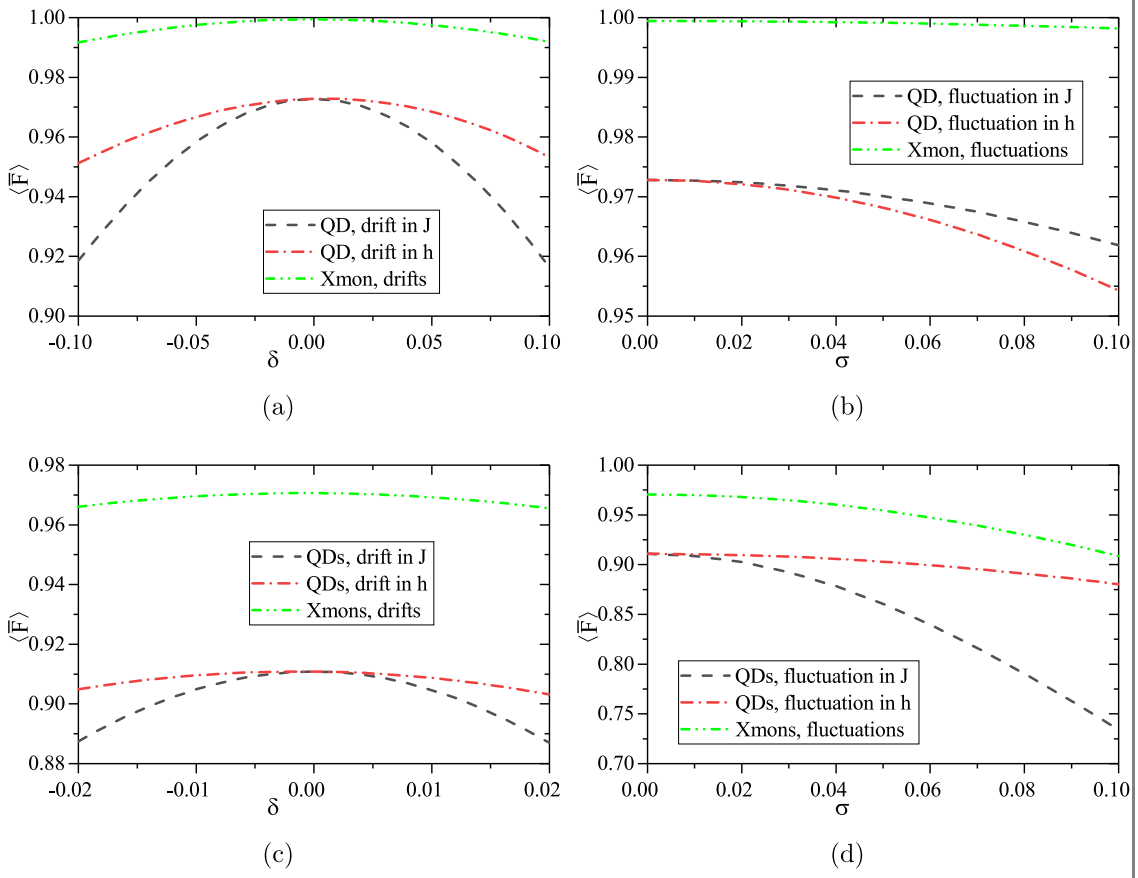

Figure 5. Average fidelities of the universal state preparation with RG algorithm over all preparing tasks versus amplitudes of different imperfections: (a) and (b) the static drifts and dynamic fluctuations in the parameters of single-qubit in semiconductor QD system and superconducting Xmon. (c) and (d) The static drifts and dynamic fluctuations in the parameters of two-qubit in semiconductor QDs system and superconducting Xmons.

3.3. Universal state preparation in noisy environment

In the previous two subsections, we have explored the performance of our scheme in realizing the universal state preparation neglecting the effects of noises stemming from the surrounding environment and errors arising from systemic imperfections. Now we turn our attention to the robustness of this approach against various adverse factors.

There are many manifestations of imperfections, and we roughly categorize them into two classes: the static drifts and the dynamic fluctuations. Their impact on the evolution of the system can be taken into account by substituting the pertaining control parameter f with the control-noise term $f+\delta$ or $f+\delta(t)$ in the corresponding Hamiltonian, respectively. The static drifts could be brought about by the misaligned control field or constant disturbance from the environment. While the dynamic fluctuations may originate from various time-dependent random control errors and stochastic noises from the environment, such as the no-zero bandwidth of the microwave drive and the charge noises arising from the uncontrolled impurities in the host material [47, 51, 52]. Regardless of their individual statics, these dynamic fluctuations will in concert behave as a noise with normal distribution for the central limit theorem [49]. At each time step the amplitude of the dynamic noise term $\delta(t)$ will be sampled from a zero-mean normal function $N(0,\sigma)$, where σ represents the standard deviation and indicates the amplitude of the noise in a sense. For simplicity, the noise term will be kept constant within a time step. We stress here that the noise term is added to the Hamiltonian after the control pulse consequence has been designed to study the performance of our scheme in face of unpredictable noises. The robustness of our scheme is verified by evaluating the average fidelity $\langle\overline{F}\rangle$ over all of the sampled preparing tasks under different types and strengths of imperfections.

For the single-qubit state preparation, the average fidelity $\langle\overline{F}\rangle$ versus the amplitudes of various static drifts and dynamic noises are plotted in figures 5(a) and (b), respectively. The impacts of time-dependent errors and noises applied to the QD's exchange coupling J and Zeeman energy gap h are investigated individually. Yet their impacts on Xmon are discussed together for simplicity, i.e. the strengths of imperfections applied to Xmon' control parameters are identified. From figures 5(a) and (b), we can see

that the average fidelity in the QD system is most affected by the static drift in J and the dynamic fluctuation in h. While for the superconducting Xmon qubit, overall, the high average fidelity is well maintained even when the system is faced with comparable noises and errors as in the QD system.

For the two-qubit state preparation, we make the assumption that the static drifts on each qubit are identical, i.e. $\delta_1 = \delta_2$ where the subscript refers to the corresponding qubit; while the dynamic noises on two qubits are different, i.e. $\delta_1(t) \neq \delta_2(t)$ where each $\delta(t)$ is sampled from the same normal function $N(0, \sigma)$ individually. The average fidelity $\langle \overline{F} \rangle$ of two considered systems as a function of the magnitude of static and dynamic imperfections is showed in figures 5(c) and (d) respectively. It is obvious that the impact of the static drifts to the systems is similar to the case of single-qubit. However, for the two-qubit QDs system, it is more affected by the dynamic fluctuation in J compared to the single-qubit case.

From the above analysis, we can conclude that, overall, these control trajectories designed by our scheme exhibit a robustness against various errors and noises.

Given the limitations of quantum computing hardware presently accessible, we simulate quantum computing on a classical computer and generate the corresponding data. Our algorithms are implemented with PYTHON 3.7.9 and QuTip 4.5.0, and have been run on a 64-core 3.40 GHz CPU with 125.6 GB memory. Details of the running environment of the algorithm can be found in the data availability statement.

4. Conclusion

Precise and universal preparation of single- and two-qubit states is fundamental to quantum information and quantum computation. Yet the difficulty of designing control trajectory in complicated systems hinders the access to optimal solution for the driving between arbitrary quantum states. In this work, based on the SG algorithm, we proposed a revised version, RG, to address this intractable problem. As demonstrations of our scheme, we apply it to the control of single- and two-qubit in the context of semiconductor DQDs and superconducting circuits and discovered a well performance, revealing its potential applicability. Compared with the typical numerical optimizations, our RG algorithm overcomes the local optimality and achieves a higher preparation quality. It is also demonstrated that the runtime of designing suited pulses with our scheme rivals to the GRAPE, which implies an outstanding efficiency. It outperforms the emerging machine learning approach with well accessibility: could tailor the proper control trajectory to drive arbitrary initial state to other arbitrary target one without any training but only at a little cost of trial and error. We also discover that the control trajectories generated by our scheme are robust against various static and dynamic imperfections. As a radically different approach from previous methods, our scheme finds a new route to achieve quantum control optimization.

5. Models

Among the numerous promising qubit modalities, semiconductor quantum dots [47, 53–61] and superconducting circuits [49, 62–71] have captured the imagination of the research field and become the leading candidates for their desirable merits, e.g. high scalability, long coherence time and desirable integration with well-established microfabrication. In this section, we introduce four models of single- and two-qubit in semiconductor DQDs and superconducting circuits.

5.1. Singlet–triplet qubits in semiconductor double quantum dots

There are many types of qubit have been proposed and demonstrated experimentally in semiconductor quantum dots, such as the spin or charge degrees of the electrons and donor nucleus [55, 57, 59–61, 72]. Due to the merit that it can be driven all electrically, the S–T_0 qubit in DQDs captures the most attention [50, 73, 74]. It is encoded by the spins of two electrons trapped in the potential created by charged electrodes on the surface of the heterostructure [55].

The effective Hamiltonian of a single S–T_0 qubit driven by external control field can be written as [47, 59, 72, 75, 76]

$$H(t) = J(t)\sigma_z + h\sigma_x, \tag{3}$$

under the computational basis $\{|0\rangle, |1\rangle\}$, where $|0\rangle = |S\rangle = (|\uparrow\downarrow\rangle - |\downarrow\uparrow\rangle)/\sqrt{2}$, $|1\rangle = |T_0\rangle = (|\uparrow\downarrow\rangle + |\downarrow\uparrow\rangle)/\sqrt{2}$. h represents the Zeeman energy gap caused by local inhomogeneous micromagnetic field. Considering that for the micromagnetic field resulted by an integrated micromagnet, h is hardly to vary during runtime, we therefore assume it as a constant and set $h = 1$ here [50]. We also take the reduced Planck constant $\hbar = 1$ throughout this work. The Pauli matrices σ_x, σ_y and σ_z indicate rotations about the x-, y- and z-axes of the Bloch sphere respectively. The exchange coupling $J(t)$ is the only

tunable parameter in this model and can be modulated with electric pulses. In addition, it is physically restricted to be non-negative and bounded.

The properties of superposition of basis states and entanglement between multiple qubits are the source of the magic of quantum computing. In semiconductor DQDs, the interaction Hamiltonian of two entanglement qubits based on Coulomb interaction reads [32, 48, 73, 74]

$$H_{2-\text{qubit}} = \frac{\hbar}{2}\begin{pmatrix} J_1+J_2 & h_2 & h_1 & 0 \\ h_2 & J_1-J_2 & 0 & h_1 \\ h_1 & 0 & J_2-J_1 & h_2 \\ 0 & h_1 & h_2 & -J_1-J_2+2J_{12} \end{pmatrix}, \tag{4}$$

under the basis constituted by $\{|SS\rangle, |ST_0\rangle, |T_0S\rangle, |T_0T_0\rangle\}$. h_i and J_i are the Zeeman energy gap and exchange interaction with the subscript $i = 1, 2$ referring to the corresponding qubit. The coupling strength between two qubits $J_{12} \propto J_1J_2$. To maintain the entanglement between two qubits, it has to keep $J_i > 0$. We set $h_1 = h_2 = 1$ and $J_{12} = J_1J_2/2$ here for simplicity.

5.2. Superconducting quantum circuits qubits

As a kind of 'artificial atom', the Hamiltonian of superconducting qubits can be designed just by tailoring the capacitance, inductance and Josephson energy [65]. According to the degrees of freedom and the ratio of Josephson energy to charging energy, superconducting qubits can mainly be classified into three categories: charge qubits [62], flux qubits [77] and phase qubits [78, 79]. Based on the above three archetypes, a variety of new types of superconducting qubits emerges, such as Transmon [80], Xmon [41, 42, 81], Gmon [82] and so on. Considering the representativeness of the Xmon type superconducting qubits, we take it as an example here. Nonetheless, this control scheme is also applicable to other superconducting qubit models.

When the qubit resonates with the microwave drive, the Hamiltonian of a single Xmon qubit in the rotating frame can be written as [41, 42, 49, 83]

$$H = \frac{\hbar}{2}A(\cos\,\phi\sigma_x + \sin\,\phi\sigma_y), \tag{5}$$

where A and ϕ are the amplitude and phase of the microwave, respectively. Obviously, when $\phi = 0$, $H = \frac{\hbar}{2}A_x\sigma_x$; in contrast, when $\phi = \pi/2$, $H = \frac{\hbar}{2}A_y\sigma_y$. Thus, the rotations about the x- and y-axes of the Bloch sphere can be obtained by properly setting A, ϕ and the duration τ of the microwave. In addition, the operation about the z-axis can be implemented physically by adjusting the current flowed into the superconducting quantum interference device loop through the so-called Z-line and the Hamiltonian can be expressed as [49, 83]

$$H = -\frac{\hbar}{2}A_z\sigma_z, \tag{6}$$

when the XY microwave drive is absent. A_z is determined by the structure of the qubit as well as the current intensity and is bounded to be nonnegative and finite.

For two capacitively coupled Xmon qubits with same frequency, using rotating-wave approximation, the additional interaction term can be written as [49, 65, 83]

$$H_{\text{couple}} = \hbar g(\sigma_1^+\sigma_2^- + \sigma_1^-\sigma_2^+), \tag{7}$$

where $\sigma_j^{\pm} = \frac{1}{2}(\sigma_x^j \pm i\sigma_y^j)$ with the superscript $j \in \{1, 2\}$ referring to the corresponding qubit. g is the coupling strength and we set $g = 1$ here.

Acknowledgments

This work was supported by the Natural Science Foundation of China (Grant Nos. 11475160, 61575180), and the Natural Science Foundation of Shandong Province (Grant No. ZR2014AM023). The author Run-hong He would also like to personally thank Jing-Hao Sun and Chen-Chen for useful discussions.

Data availability statement

The data that support the findings of this study are openly available at the following URL/DOI: https://gitee.com/herunhong/USP-via-RG [84].

ORCID iDs

Run-Hong He https://orcid.org/0000-0002-1387-1468
Zhao-Ming Wang https://orcid.org/0000-0002-8976-9515

References

[1] Nielsen M A and Chuang I L 2010 *Quantum Computation and Quantum Information* 10th Anniversary Edition (Cambridge: Cambridge University Press)
[2] Bishnoi B 2020 Quantum-computation and applications (arXiv:2006.02799)
[3] Shor P W 1994 Algorithms for quantum computation: discrete logarithms and factoring *Proc. of 35th Annual Symp. on the Foundations of Computer Science* (USA: IEEE Computer Society Press) pp 124–4
[4] Feynman R P 1999 Simulating Physics with Computers *Feynman and Computation: Exploring the Limits of Computers* (USA: Perseus Books)
[5] Georgescu I M, Ashhab S and Nori F 2014 Quantum simulation *Rev. Mod. Phys.* **86** 153–85
[6] Grover L K 1996 A fast quantum mechanical algorithm for database search (arXiv:quant-ph/9605043)
[7] Farhi E, Goldstone J and Gutmann S 2014 A quantum approximate optimization algorithm (arXiv:1411.4028)
[8] Wang S B, Wang Z M, Li W D, Fan L X, Cui G L, Wei Z Q and Gu Y J 2020 A quantum Poisson solver implementable on NISQ devices (arXiv:2005.00256v2)
[9] Vandersypen L M K and Chuang I L 2005 NMR techniques for quantum control and computation *Rev. Mod. Phys.* **76** 1037
[10] Bellec M, Nikolopoulos G M and Tzortzakis S 2012 Faithful communication Hamiltonian in photonic lattices *Opt. Lett.* **37** 4504–6
[11] Perez-Leija A, Keil R, Moya-Cessa H, Szameit A and Christodoulides D N 2013 Perfect transfer of path-entangled photons in Jxphotonic lattices *Phys. Rev.* A **87** 022303
[12] Richerme P, Gong Z-X, Lee A, Senko C, Smith J, Foss-Feig M, Michalakis S, Gorshkov A V and Monroe C 2014 Non-local propagation of correlations in quantum systems with long-range interactions *Nature* **511** 198–201
[13] Yung M-H, Casanova J, Mezzacapo A, McClean J, Lamata L, Aspuru-Guzik A and Solano E 2014 From transistor to trapped-ion computers for quantum chemistry *Sci. Rep.* **4** 3589
[14] Childress L and Hanson R 2013 Diamond NV centers for quantum computing and quantum networks *MRS Bull.* **38** 134–8
[15] Schirhagl R, Chang K, Loretz M and Degen C L 2014 Nitrogen-vacancy centers in diamond: nanoscale sensors for physics and biology *Annu. Rev. Phys. Chem.* **65** 83
[16] Dai H N, Yang B, Reingruber A, Sun H, Xu X F, Chen Y A, Yuan Z S and Pan J W 2017 Four-body ring-exchange interactions and anyonic statistics within a minimal toric-code Hamiltonian *Nat. Phys.* **13** 1195–200
[17] Mottonen M, Vartiainen J J, Bergholm V and Salomaa M M 2004 Quantum Circuits for General Multiqubit Gates *Phys. Rev. Lett.* **93** 130502
[18] Nakajima Y, Kawano Y and Sekigawa H 2005 A new algorithm for producing quantum circuits using KAK decompositions (arXiv:quant-ph/0509196v4)
[19] Williams C P and 2011 *Explorations in Quantum Computing* Second Edition (London: Springer)
[20] Vatan F and Williams C 2004 Optimal quantum circuits for general two-qubit gates *Phys. Rev.* A **69** 32315
[21] Chong F T, Franklin D and Martonosi M 2017 Programming languages and compiler design for realistic quantum hardware *Nature* **549** 180–7
[22] Paler A, Polian I, Nemoto K and Devitt S J 2015 Fault-tolerant, high-level quantum circuits: form, compilation and description *Quantum Sci. Technol.* **2** 025003
[23] Wang X, Bishop L S, Barnes E, Kestner J P and Das Sarma S 2014 Robust quantum gates for singlet–triplet spin qubits using composite pulses *Phys. Rev.* A **89** 022310
[24] Wang X, Bishop L S, Kestner J P, Barnes E, Sun K and Das Sarma S 2012 Composite pulses for robust universal control of singlet–triplet qubits *Nat. Commun.* **3** 997
[25] Throckmorton R E, Zhang C, Yang X-C, Wang X, Barnes E and Das Sarma S 2017 Fast pulse sequences for dynamically corrected gates in singlet–triplet qubits *Phys. Rev.* B **96** 195424
[26] Yang X-C, Yung M-H and Wang X 2018 Neural-network-designed pulse sequences for robust control of singlet–triplet qubits *Phys. Rev.* A **97** 042324
[27] Zhang X M, Wei Z, Asad R, Yang X C and Wang X 2019 When reinforcement learning stands out in quantum control? a comparative study on state preparation *Npj Quantum Information* **5** 85
[28] Zheng A and Zhou D L 2019 Deep reinforcement learning for quantum gate control *Europhys. Lett.* **126** 60002
[29] Niu M Y, Boixo S, Smelyanskiy V and Neven H 2019 Universal quantum control through deep reinforcement learning *npj Quantum Information* **5** 33
[30] Lin J, Lai Z Y and Li X 2020 Quantum adiabatic algorithm design using reinforcement learning *Phys. Rev.* A **101** 052327
[31] Wang Z T, Ashida Y and Ueda M 2020 Deep reinforcement learning control of quantum cartpoles *Phys. Rev. Lett.* **125** 190404
[32] He R H, Wang R, Wu J, Nie S S, Zhang J H and Wang Z M 2021 Deep reinforcement learning for universal quantum state preparation via dynamic pulse control (arXiv:2012.00326)
[33] Haug T, Mok W K, You J B, Zhang W, Png C E and Kwek L C 2021 Classifying global state preparation via deep reinforcement learning *Mach. Learn.: Sci. Technol.* **2** 01LT02
[34] Ferrie C 2014 Self-guided quantum tomography *Phys. Rev. Lett.* **113** 190404

[35] Khaneja N, Reiss T, Kehlet C, Schulte-Herbrüggen T and Glaser S J 2005 Optimal control of coupled spin dynamics: design of NMR pulse sequences by gradient ascent algorithms *J. Magn. Reson.* **172** 296–305
[36] Rowland B and Jones J A 2012 Implementing quantum logic gates with gradient ascent pulse engineering: principles and practicalities *Phil. Trans. R. Soc.* A **370** 4636–50
[37] Doria P, Calarco T and Montangero S 2011 Optimal control technique for many body quantum systems dynamics *Phys. Rev. Lett.* **106** 237–51
[38] Caneva T, Calarco T and Montangero S 2011 Chopped random-basis quantum optimization *Phys. Rev.* A **84** 022326
[39] Cormen T, Leiserson C and Rivest R 2001 *Introduction to Algorithms* Second Edition (London: The MIT Press)
[40] Balaman Y 2019 Chapter 6 - Basics of Decision-Making in Design and Management of Biomass-Based Production Chains *Decision-Making for Biomass-Based Production Chains* (New York: Academic) https://doi.org/10.1016/B978-0-12-814278-3.00006-6
[41] Barends R *et al* 2013 Coherent Josephson qubit suitable for scalable quantum integrated circuits *Phys. Rev. Lett.* **111** 32–6
[42] O'Malley P J J *et al* 2016 Scalable quantum simulation of molecular energies *Phys. Rev.* X **6** 031007
[43] Sutton R S and Barto A G 2015 *Reinforcement Learning: An Introduction* Second Edition (Cambridge, MA: MIT Press)
[44] Zahedinejad E, Ghosh J and Sanders B C 2015 High-fidelity single-shot toffoli gate via quantum control *Phys. Rev. Lett.* **114** 200502
[45] Egger D J and Wilhelm F K 2013 Optimized controlled-z gates for two superconducting qubits coupled through a resonator *Supercond. Sci. Technol.* **27** 014001
[46] Guerreschi G G and Park J 2018 Two-step approach to scheduling quantum circuits *Quantum Sci. Technol.* **3** 045003
[47] Petta J R *et al* 2005 Coherent manipulation of coupled electron spins in semiconductor quantum dots *Science* **309** 2180–4
[48] Shulman M D, Dial O E, Harvey S P, Bluhm H, Umansky V and Yacoby A 2012 Demonstration of entanglement of electrostatically coupled singlet–triplet qubits *Science* **336** 202–5
[49] Krantz P, Kjaergaard M, Yan F, Terry P, Orlando , Gustavsson S and Oliver W D 2019 A quantum engineer's guide to superconducting qubits (arXiv:1904.06560)
[50] Wu X *et al* 2014 Two-axis control of a singlet–triplet qubit with an integrated micromagnet *Proc. Natl Acad. Sci.* **111** 11938–42
[51] Barnes E, Cywiński Ł and Das Sarma S 2012 Nonperturbative master equation solution of central spin dephasing dynamics *Phys. Rev. Lett.* **109** 140403
[52] Nguyen N and Sarma S D 2011 Impurity effects on semiconductor quantum bits in coupled quantum dots *Phys. Rev.* B **83** 235322
[53] Jang W, Cho M-K, Kim J, Chung H, Umansky V and Kim D 2020 Three individual two-axis control of singlet–triplet qubits in a micromagnet integrated quantum dot array (arXiv:2009.13182)
[54] Watson T F *et al* 2018 A programmable two-qubit quantum processor in silicon *Nature* **555** 633–7
[55] Zajac D M, Sigillito A J, Russ M, Borjans F, Taylor J M, Burkard G and Petta J R 2018 Resonantly drivenCNOT gate for electron spins *Science* **359** 439–42
[56] Huang W *et al* 2019 Fidelity benchmarks for two-qubit gates in silicon *Nature* **569** 532–6
[57] Loss D and Divincenzo D P 1997 Quantum computation with quantum dots *Phys. Rev.* A **57** 120–6
[58] Bluhm H, Foletti S, Neder I, Rudner M, Mahalu D, Umansky V and Yacoby A 2010 Dephasing time of GaAs electron-spin qubits coupled to a nuclear bath exceeding 200 μs *Nat. Phys.* **7** 109–13
[59] Maune B M *et al* 2012 Coherent singlet–triplet oscillations in a silicon-based double quantum dot *Nature* **481** 344–7
[60] Zhang X, Li H O, Cao G, Xiao M, Guo G C and Guo G P 2019 Semiconductor quantum computation *Natl Sci. Rev.* **6** 32–54
[61] Zhang X, Li H O, Wang K, Cao G, Xiao M and Guo G P 2018 Qubits based on semiconductor quantum dots *Chin. Phys.* B **27** 020305
[62] Nakamura Y, Pashkin Y A and Tsai J S 1999 Coherent control of macroscopic quantum states in a single-cooper-pair box *Nature* **398** 786–8
[63] Gibney E 2019 Quantum supremacy using a programmable superconducting processor *Nature* **574** 505–10
[64] Devoret M H and Schoelkopf R J 2013 Superconducting circuits for quantum information:An outlook *Science* **339** 1169–74
[65] Wendin G 2017 Quantum information processing with superconducting circuits: a review *Rep. Prog. Phys.* **80** 106001
[66] Kjaergaard M, Schwartz M E, Braumüller J, Krantz P and Oliver W D 2020 Superconducting qubits: current state of play *Annu. Rev. Condens. Matter Phys.* **11** 369–95
[67] Kockum A F and Nori F 2019 Quantum bits with Josephson junctions (arXiv:1908.09558)
[68] Clarke J and Wilhelm F K 2008 Superconducting quantum bits *Nature* **453** 1031–42
[69] Song C *et al* 2017 10-qubit entanglement and parallel logic operations with a superconducting circuit *Phys. Rev. Lett.* **119** 180511
[70] Gong M *et al* 2021 Quantum walks on a programmable two-dimensional 62-qubit superconducting processor *Science* **372** 948-52
[71] Wu Y *et al* 2021 Strong quantum computational advantage using a superconducting quantum processor (arXiv:2106.14734)
[72] Jeremy L 2002 Universal quantum computational with spin-1/2 pairs and heisenberg exchange *Phys. Rev. Lett.* **89** 147902
[73] Taylor J M, Engel H-A, Dür W, Yacoby A, Marcus C M, Zoller P and Lukin M D 2005 Fault-tolerant architecture for quantum computation using electrically controlled semiconductor spins *Nat. Phys.* **1** 177–83
[74] Nichol J M, Orona L A, Harvey S P, Fallahi S, Gardner G C, Manfra M J and Yacoby A 2017 High-fidelity entangling gate for double-quantum-dot spin qubits *npj Quantum Information* **3** 3
[75] Malinowski F K *et al* 2017 Notch filtering the nuclear environment of a spin qubit *Nat. Nanotechnol.* **12** 16–20
[76] Foletti S *et al* 2009 Universal quantum control of two-electron spin quantum bits using dynamic nuclear polarization *Nat. Phys.* **5** 903–8
[77] Mooij J E 1999 Josephson persistent-current qubit *Science* **285** 1036-9
[78] Martinis J M 2009 Superconducting phase qubits *Quantum Inf. Process.* **8** 81–103
[79] Neeley M *et al* 2010 Generation of three-qubit entangled states using superconducting phase qubits *Nature* **467** 570–3
[80] Koch J, Yu T M, Gambetta J, Houck A A and Schoelkopf R J 2007 Charge insensitive qubit design derived from the cooper pair box *Phys. Rev.* A **76** 042319
[81] Kelly J *et al* 2015 State preservation by repetitive error detection in a superconducting quantum circuit *Nature* **519** 66–9
[82] Chen Y 2014 Qubit architecture with high coherence and fast tunable coupling *Phys. Rev. Lett.* **113** 220502
[83] Huang H, Wu D, Fan D and Zhu X 2020 Superconducting quantum computing: a review (arXiv:2006.10433v3)
[84] He R-H 2021 Data and code for universal quantum state preparation via RG https://gitee.com/herunhong/USP-via-RG